Diagnostic Function of 3D Optical Coherence Tomography Multimode Images in Diagnosis of Acute Central Serous Chorioretinopathy

Gui-ling Zhao
Guangdong Medical University
Rui-zhuang Li
Guangdong Medical University
Yan-hua Pang
Guangdong Medical University
Xiu-qin Wang
Guangdong Medical University
Jin-fen Wei
Guangdong medical university
Zhou Zhou
Guangdong medical university
Jing-xiang Zhong (zhongjing.optic@gmail.com)
Jinan University First Affiliated Hospital https://orcid.org/0000-0003-3204-5329

Research article

Keywords: Imaging, three-dimensional (3D), Optical coherence tomography (OCT), Central serious chorioretinopathy (CSC), ILM-RPE thickness map, Shadowgram, RPE surface

Posted Date: December 29th, 2020

DOI: https://doi.org/10.21203/rs.3.rs-134896/v1

Abstract

Background: Spectral-Domain Optical coherence tomography (SD-OCT) provides non-invasive, high speed, high resolution, three-dimensional cross-section imaging of macula. This study was aimed to investigate the diagnostic value of multimodal imaging technique of three-dimension (3D) optical coherence tomography (OCT) (3D-OCT) for diagnosis and characterizing of acute central serous chorioretinopathy (CSC).

Methods: The 3D-OCT examinations of 82 cases of acute CSC were performed on the macular area, and the image characteristics were analyzed. Our study included a total of 87 eyes from 82 cases of CSC patients, 67 males and 15 females, aged 27 to 56 years, mean age 42.89±7.80 years old.

Results: According to B-scan images, 87 (100%) eyes had ERD, 38 (44%) eyes had bulge of RPE, 36 (41%) eyes had PED, 8 (9%) eyes had membrane -like structure, 2 (2%) eyes had subretinal dot-like precipitates, 1 (1%) eyes had focal choroidal excavation (FCE), and 1 (1%) eye had fluctuation of internal limiting membrane (FI). In ILM-RPE thickness map, all eyes had a round or round like regular uniform domes. Total of 57 (66%) domes were limited in exam area and 30 (44%) domes beyond the scope of this examination and only part of the dome could be observed. In the Shadowgram image, all eyes had a round or round like black figure that correspond with domes In ILM-RPE thickness map. In RPE surface, 76(87%) eyes had a shallow plate depression, 71(82%) had small focal uplift and 1 (1%) eye had a focal concave.

Conclusions: In OCT ILM-RPE thickness map, Shadowgram, and RPE surface, acute CSC had special images and can be helpful for diagnosis and difference diagnosis.

Trial registration: Not applicable.

1. Background

Central serous chorioretinopathy (CSC) or central serous retinopathy (CSR) is a common disease, characterized by serous detachment of the neurosensory retina and/or the retinal pigment epithelium (RPE) that often involves the macula. The hallmark of CSC is the accumulation of subretinal fluid between the neurosensory retina and the RPE.

The alteration in choroidal circulation is probably the main mechanism leading to the development of CSC. High choroidal vascular permeability leads to increased hydrostatic pressure under RPE, which in turn destroys the integrity of RPE (1). The fluid in the choroid enters sub-retina through the damaged RPE, resulting in fluid accumulation under the retina (2).

The diagnosis of CSC is made by fundus exam combined with imaging of the retina and choroid with optical coherence tomography (OCT), fluorescein angiography (FA), indocyanine green angiography (ICGA), or combinations of these imaging techniques. FA allow for the identification of abnormal leakage of fluid from the choroidal and retinal vessels as well as through the RPE layer. FA of CSC typically shows a focal area of leakage of the dye from the RPE into the subretinal space with two main patterns: “ink blot” or “a smoke-stack” (3). The inkblot pattern of leakage was relatively more common than smokestack pattern. In most cases, the dye slowly leaks symmetrically in all directions, eventually fulling the entire retina detached. There are one or two leakage points in common, but in some cases it can be up seven or more points. There may be no clear leakage, but diffuse intense fluorescence. Half of the leakage occurred in the nasal side retina, and about 35% appeared on the temporal side (4, 5).

Spectral-Domain Optical coherence tomography (SD-OCT) provides non-invasive, high speed, high resolution, three-dimensional cross-section imaging of macula. It is widely used for investigation and diagnosis of macular diseases. In addition to conventional tomographic B-Scan, OCT now provides multiple 3D model reports such as ILM-RPE thickness, RPE surface, and shadowgram. We have found that OCT's multiple 3D model images are an important complement to the B-Scan model. OCT is noninvasive and fast and we hope that OCT can replace FFA to the greatest extent and most patients can be diagnosed by OCT only. Previous literature has described the OCT performance of CSC, each article has its own characteristics and focus (6–8). We carefully analyze the images of 3D-OCT of typical CSC, and have some new understanding of the OCT characteristics.

2. Methods

2.1 Subjects

We included acute CSC patients who were treated at the outpatient clinic or hospitalized from January 2016 to December 2018. The chief complaint was blurred vision, dimmed vision, diminished vision, and deformed vision. The initial symptoms lasted less than 3 months. Single or multiple circular prominences at the posterior pole were detected and OCT examinations revealed neurosensory retinal detachment. The exclusion criteria of the study were: patients with high myopia or blurred vision caused by other conditions, incomplete or missing data, a history of trauma or eye surgeries, and patients with atypical clinical manifestations or uncertain diagnosis.

2.2 General examinations

Routine eye examinations, slip lamp tests, fundus examinations, and non-contact tonometry were performed. FFA, and other eye or systemic examinations were performed if necessary.

2.3 Macular OCT

The Topcon 3D -1000 OCT was used to detect ocular structures at a wavelength of 840 nm. Axial and lateral resolutions were set to 5 μm and 20 μm, respectively. Scans were made at a speed of 18000 A/s, a depth of 2.0 mm, and a range of 6 × 6 mm. Macular thickness was analyzed in 3D macular mode.

The parameter values were calculated automatically. We analyzed 64 horizontal B-scan images, retinal thickness maps (ILM-RPE), shadowgram, and RPE surface. Different intensities of light signals and retinal thicknesses were represented in OCT images on a rainbow color scale. In the B-scan images, tissue color indicated reflection intensity. The following colors represented reflected light intensity in decreasing order: red, orange, green, blue, and black. Black indicted the tissue with the weakest light reflection (Fig. 1A).

Retinal thickness was defined and determined as the distance between internal limiting membrane (ILM) to the RPE. The ILM-RPE maps were generated within a range of 6 × 6 mm in the center of the retina. Thickness was represented by pseudocolors, with white corresponding to the greatest thickness. White, red, orange, yellow, green, and blue indicated successively decreasing levels of thickness. ILM contour maps and RPE surface maps were reconstructed with using computer software (Fig. 1B).

Shadowgram is a plane image obtained by two-dimensional processing of multiple B-Scan axial images (64 in this study) according to the intensity of reflected light. It is shown in black-and-white images, similar to black-and-white photographs taken with infrared light. Normal Shadowgram is white or grayish-white, with a grayish-black dot in the fovea, a brighter parafovea, and a clear image of retinal blood vessels (Fig. 1C). The gray level changes when abnormal.

RPE surface is the synthesized image of each point automatically recognized by the computer RPE. Normal RPE surface is smooth and horizontal slightly curved (Fig. 1D).

3. Results

3.1 Baseline information

Eighty two VKH patients with 87 eyes were included (67 males, 15 females, aged 27 to 56 years old, with mean age of 42.89 ± 7.80 years). They sought medical care at our hospital at 2 to 30 days (mean 16.63 ± 11.2 days) after onset. Five cases were affected in bilateral eyes, and 77 cases were affected in only one eye.

3.2 B-scan images of macula

Of the OCT B-scan images, 87 (100%) eyes had ERD, 38 (44%) eyes had bulge of RPE (Fig. 2A), 36 (41%) eyes had PED (Fig. 2B), 8 (9%) eyes had membrane -like structure (Fig. 2C), 2 (2%) eyes had Subretinal dot-like precipitates (Fig. 2D), 1 (1%) eyes had FCE (Fig. 2E)and 1 (1%) eye had FI (Fig. 2F).

3.3 ILM-RPE map

In ILM-RPE thickness map, all eyes had a round or round like regular uniform dome. Fifty seven (66%) domes were limited in 6 × 6 mm^2 exam area and 30 (44%) domes Beyond the scope of this examination and only part of the dome can be seen (Fig. 3).

ILM-RPE map also showed small circular dot-like changes. The color of the dot was different from that of the surrounding area. The color of the dot was colder in 42 eyes than that of the surrounding area, indicating that the ILM-RPE thickness of the dot position was smaller than that of the surrounding area (Fig. 4A, B); the opposite was observed in one eye (Fig. 4C, D).

3.4 Shadowgram

In Shadowgram image, all eyes had a round or round like black figure that correspond with domes In ILM-RPE thickness map (Fig. 5).

3.5 RPE surface

In RPE surface, 76 (87%) eyes had a shallow plate depression, 71 (82%) had small focal uplift and 1 (1%) eye had a focal concave (Fig. 6).

4. Discussion

Central serous chorioretinopathy (CSC) is an idiopathic disease of the posterior pole of the retina, which often appears as serous retinal detachment accompanied by leakage of altered retinal pigment epithelium (RPE). Mechanical stress resulting from increased intra-choroidal pressure reduces RPE adhesion and alters hydro-ionic RPE regulation, which in turn causes PED. EDR is often associated with a mechanical abrasion resulting from an active flow through a break in the RPE.

The most common manifestation of B-Scan imaging in acute CSC is ERD. The neurosensory of retina uplift, there is a dark area of fluid accumulation beneath it. A high reflective light band at the bottom is the retinal pigment epithelial layer. Most reports mention the presence of ERD (9, 10), 100% of our patients have this sign. Most of the ERD areas of CSC are non-reflective dark areas, but there are few reports of membrane-like structure (11). Our study found that nearly 10% of the patients had this characteristic. CSC's membrane -like structure is localized, well-defined, and has some relationship with PED or RPE protuberances (12, 13). Fujimoto et al. (14) Study the leakage point of CSC found that half of the leakage point has a membrane-like structure. Many studies hold the view on the membrane -like structure of CSC as cellulose exudation. We hypothesized that the membrane -like structure in CSC should also be associated with local inflammation,

We found dot-like precipitates in two eyes in the retinal neurosensory detachment area of CSC. It has been reported that up to 65% of the EDR areas of CSC eyes have precipitates (15, 16). This neoplasm can be attached to the retina or in the retinal detachment area (17, 18). There is a lot of speculation about this precipitates. The main idea is that the outer segment of the photoreceptor cells precipitates in the subretinal space. It may also be the accumulation of fibrin or lipid, and the macrophages that remove these debris.

PED is the separation of the RPE from Bruch's membrane or choroid membrane. Upon OCT, PED usually manifests as dome-shaped RPE protrusions stretching towards the retina, usually with a uniform low reflection area behind it (19, 20). PED is very common in CSC, and sometimes occurs with ERD, and sometimes it appears separately (20). RPE bulges, sometimes described as rough RPE (19), show slight protrusions in the RPE layer, with no clear low-reflex region behind them (21). This small bulge is common in CSC. Montero et al. (22) reported this small bulge in 35 of 39 eyes, but most of the reports were 30‒40% (21, 23). PED and bulge were both associated with the leakage point found by FFA examination (10, 14). Some people believed that bulge was associated with hyperplasia of pigment epithelium (21). On OCT images, we found that some bulges were not distinguishable from PEDs, and we speculated that some bulges were small PEDs.

Focal choroidal excavation (FCE) is a newly discovered disease. In 2006, Jampol et al. (24) first reported a case of choroidal excavation found in time domain OCT. In 2010, Abe et al. and Wakabayashi et al. (25, 26) reported 4 cases of monocular focal choroidal excavation with SD-OCT. Among the 3 cases reported by Wakabayashi et al. (26), there were two lesions in one eye. Margolis et al. (27) reviewed the focal choroidal excavation in 12 patients and named it focal choroidal excavation (FCE) defined as macular area Choroidal excavation, without posterior staphyloma or scleral bulge, without trauma, uveitis, retinal or choroidal vascular disease or infection, and had been divided into two types, conforming focal choroidal excavation C-FCE and nonconforming focal choroidal excavation NC-FCE. In the former, the top of photoreceptor cells and retinal pigment epithelium were not separated, the photoreceptor cell layer was thicker than that in the area not affected by depression, and the junction between inner and outer segments and pigment epithelium were not disturbed. In NC-FCE, the top of the photoreceptor is separated from the posterior RPE, accompanied by a low reflex region that may represent the subretinal serum. In these types, the pigment epithelium and inner segment/ outer segment connections are usually disturbed. Then Katome et al. reported two cases of C-FCE detected by EDI-OCT in three eyes in 2012 (28), one of which was binocular with two lesions in the left eye and the other with choroidal neovascularization (CNV). Kobayashi et al. (29) also reported a case of NC-FCE with CNV. Say et al. (30) reported a case of subretinal hemorrhage at the infratemporal arch with macular involvement. The report on FCE gradually increased (31, 32). In the study of CSC and FCE, Wang et al. (31), 17 cases (19 eyes, 21 FCEs) were found in 351 patients with CSC. The etiology of FCE is not clear. The latest study suggests that choroidal abnormalities occur (32). They found that the FCE corresponds to an increase in the inner choroidal reflex, unclear vascular development, the outer choroidal traction by the inner choroidal cavity, visible superior choroidal cavity, choroidal scleral interface is still smooth. However, the relationship between CSC and FCE is uncertain, Liu et al. (32) and other discussions suggest that there is no final conclusion, but Wang et al. (31) believes that the abnormality of choroidal vessels in FCE is related to the occurrence of CSC.

Fluctuation of internal limiting membrane (FI) was observed in one eye. FI was found in OCT of VKH before (21, 33). Our previous studies of VKH also found FI, and speculated that there is a certain relationship with retinal Radial stripes (34). Dusheng et al. (21) speculated that FI was associated with inflammation. Considering that the inflammation of CSC was not common, we believe that this change was due to mechanical traction caused by changes in the retina and choroids.

Both ILM-RPE map and Shadowgram of OCT are similar to fundus photography in that they observe the shape of the retina directly from the front and can quickly determine the location, extent and basic shape of the lesion. They complement each other with B-Scan and are indispensable for the diagnosis of diseases.

The ILM-RPE Map feature of CSC is very obvious. The lesion is typically round or round like with some very regular shapes; the uplift is uniform, the thickest in the center, slightly thickened at the edge of the detachment zone, and then excessive to normal. This is very consistent with the appearance of CSC seen under ophthalmoscope, and the FFA examination of the dye slowly leaking symmetrically in all directions (3). In some CSC, the lesions are large or deviate from the macular center. We can see only a round-like part of the lesion in the 6×6 mm^2 range. With the improvement of OCT and the enlargement of the scope of examination, the ILM-RPE Map of OCT will be more convenient to observe CSC. The ILM-RPE Map does not show the contour of the inner limiting membrane surface, but the thickness between ILM and RPE, so the RPE uplift on the ILM-RPE Map is an excavation, and the FCE is a protrusion. The macular fovea itself is thinner and sometimes shows small excavation on the topographic map.

The Shadowgram of CSC has good contrast between black and white, it is convenient for clinical observation. Typical round or round like lesions, or part of the lesion round like, is very consistent with the scope of the lesions on ILM-RPE Map, and is very consistent with neurosensory detachment or RPE lesions. The range of lesions is easily estimated accurately.

OCT scanning light source wavelength 840 nm, belongs to infrared light, Shadowgram is similar to the black-and-white fundus photography taken with this wavelength. Zhou et al. (35) studied the NIR images of CSC with similar wavelengths (820 nm). Results Neuroepithelial detachment showed elliptical dark areas on NIR images with clear boundaries, and PED showed circular dark areas with clear boundaries on NIR images, which were consistent with fundus photography, FFA and ICGA. Comparing NIR images with OCT's Shadowgram, we found that they were very similar, but our Shadowgram had better contrast and was easier to distinguish the lesions.

RPE Surface is a surface morphology of RPE. RPE Surface of CSC shows a special shallow plate depression. This may be related to the mechanical separation of CSC's RPE and photoreceptor cells and the uniform thinning of RPE. RPE Surface's small uplift is very common in CSC, and is consistent with B-Scan's PED and bulge positions. Despite the presence of choroidal thickening (6, 36), the RPE Surface of CSC remained smooth without undulation.

5. Conclusions

Acute CSC on OCT has common changes like retinal neurosensory detachment, focal RPE processes, focal PED, there are also rare changes like the membranous reflex in the detachment area; subretinal dot-like precipitates; FCE and FI. ILM-RPE thickness map have typically round or round like domes with some very regular shapes; Shadowgram have typically round or round like lesions, and RPE surface of acute CSC had special round like images and can quickly determine the location, extent and basic shape of the lesion.

List Of Abbreviations

Spectral-Domain Optical coherence tomography (SD-OCT), three-dimension (3D), central serous chorioretinopathy (CSC), central serous retinopathy (CSR), retinal pigment epithelium (RPE), fluorescein angiography (FA), indocyanine green angiography (ICGA), internal limiting membrane (ILM), Focal choroidal excavation (FCE), choroidal neovascularization (CNV).

Declarations

Ethics approval and consent to participate:

This study was conducted according to the guidelines laid down in the Declaration of Helsinki and all procedures involving research study participants were approved by the local Human Ethics and Research Ethics committees of Affiliated Hospital of Guangdong Medical University, Zhanjiang, China (Approval No.:2017.GMU.153). Written informed consent was obtained from all patients.

Consent for publication:

This manuscript has not been published and is not under consideration for publication elsewhere in whole or in part. No conflicts of interest exist in the submission of this manuscript, and the manuscript has been approved for publication by all listed authors.

Availability of data and material:

The datasets used and/or analysed during the current study are available from the corresponding author on reasonable request.

Competing interests:

None of the authors has any financial and personal relationships with other people or organizations that could potentially and inappropriately influence this work and its conclusions. Authors declared no competing interest on publishing this paper.

Funding:

Not applicable.

Authors' contributions:

Conceptualization: GZ and JZ; Data curation: RL, YP and JW; Formal analysis: RL and ZZ; Funding acquisition: JZ; Investigation: YP and XW; Methodology: GZ; Project administration: GZ; Resources: GZ; Software: ZZ; Supervision: JZ; Validation: YP and JW; Visualization: GZ; Writing–original draft: GZ; Writing–review & editing: GZ and JZ. All authors have read and approved the manuscript.

Acknowledgements:

The authors wish to thank all members of the ophthalmology department for their great help with initial data acquisition.

References

1. Uyama M, Matsunaga H, Matsubara T, Fukushima I, Takahashi K, Nishimura T. Indocyanine green angiography and pathophysiology of multifocal posterior pigment epitheliopathy. Retina. 1999;19(1):12–21.
2. Yannuzzi LA. Central Serous Chorioretinopathy: A Personal Perspective. Vol. 149, American Journal of Ophthalmology. Elsevier Inc.; 2010. p. 361-363.e1.
3. Spitznas M, Huke J. Number, shape, and topography of leakage points in acute type I central serous retinopathy. Graefe's Arch Clin Exp Ophthalmol. 1987;225(6):437–40.
4. Shahin MM. Angiographic characteristics of central serous chorioretinopathy in an Egyptian population. Int J Ophthalmol. 2013;6(3):342–5.
5. Kitaya N, Nagaoka T, Hikichi T, Sugawara R, Fukui K, Ishiko S, et al. Features of abnormal choroidal circulation in central serous chorioretinopathy. Br J Ophthalmol. 2003 Jun 1;87(6):709–12.
6. Imamura Y, Fujiwara T, Margolis R, Spaide RF. Enhanced depth imaging optical coherence tomography of the choroid in central serous chorioretinopathy. Retina [Internet]. 2009 Nov [cited 2020 Feb 24];29(10):1469–73. Available from: http://www.ncbi.nlm.nih.gov/pubmed/19898183
7. Maruko I, Iida T, Sugano Y, Ojima A, Sekiryu T. Subfoveal choroidal thickness in fellow eyes of patients with central serous chorioretinopathy. Retina [Internet]. 2011 Sep [cited 2020 Feb 24];31(8):1603–8. Available from: http://www.ncbi.nlm.nih.gov/pubmed/21487334
8. Maruko I, Iida T, Sugano Y, Ojima A, Ogasawara M, Spaide RF. Subfoveal choroidal thickness after treatment of central serous chorioretinopathy. Ophthalmology [Internet]. 2010 Sep [cited 2020 Feb 24];117(9):1792–9. Available from: http://ovidsp.ovid.com/ovidweb.cgi?

T=JS&CSC=Y&NEWS=N&PAGE=fulltext&D=medl&AN=20472289 http://sfx.york.ac.uk/sfxlcl3?sid=OVID:medline&id=pmid:20472289&id=doi:10.1016/j.ophtha.2010.01.023&issn=0161-6420&isbn=&volume=117&issue=9&spage=1792&pages=1792-9&date=2010&title=Ophthalmology&atitle=Subfoveal+choroidal+thickness+after+treatment+of+central+serous+chorioretinopathy.&aulast=Maruko&pid=9

9. Shin YU, Lee BR. Retro-mode imaging for retinal pigment epithelium alterations in central serous chorioretinopathy. Am J Ophthalmol [Internet]. 2012 Jul [cited 2020 Feb 24];154(1):155-163.e4. Available from: http://www.ncbi.nlm.nih.gov/pubmed/22503695
10. Lehmann M, Wolff B, Vasseur V, Martinet V, Manasseh N, Sahel JA, et al. Retinal and choroidal changes observed with "En face" enhanced-depth imaging OCT in central serous chorioretinopathy. Br J Ophthalmol [Internet]. 2013 Sep [cited 2020 Feb 24];97(9):1181–6. Available from: http://www.ncbi.nlm.nih.gov/pubmed/23823080
11. Yu J, Jiang C, Xu G. Study of subretinal exudation and consequent changes in acute central serous chorioretinopathy by optical coherence tomography. Am J Ophthalmol [Internet]. 2014 Oct [cited 2020 Feb 24];158(4):752-756.e2. Available from: http://www.ncbi.nlm.nih.gov/pubmed/24973608
12. Gass JDM. Central Serous Chorioretinopathy and White Subretinal Exudation During Pregnancy. Arch Ophthalmol [Internet]. 1991 May [cited 2020 Feb 24];109(5):677–81. Available from: http://www.ncbi.nlm.nih.gov/pubmed/2025170
13. Saito M, Iida T, Kishi S. Ring-shaped subretinal fibrinous exudate in central serous chorioretinopathy. Jpn J Ophthalmol [Internet]. 2005 Nov [cited 2020 Feb 24];49(6):516–9. Available from: http://www.ncbi.nlm.nih.gov/pubmed/16365799
14. Fujimoto H, Gomi F, Wakabayashi T, Sawa M, Tsujikawa M, Tano Y. Morphologic Changes in Acute Central Serous Chorioretinopathy Evaluated by Fourier-Domain Optical Coherence Tomography. Ophthalmology [Internet]. 2008 Sep [cited 2020 Feb 24];115(9):1494–500, 1500.e1-2. Available from: http://www.ncbi.nlm.nih.gov/pubmed/18394706
15. Kon Y, Iida T, Maruko I, Saito M. The optical coherence tomography-ophthalmoscope for examination of central serous chorioretinopathy with precipitates. Retina [Internet]. 2008 Jun [cited 2020 Feb 24];28(6):864–9. Available from: http://www.ncbi.nlm.nih.gov/pubmed/18536604
16. Matsumoto H, Kishi S, Sato T, Mukai R. Fundus autofluorescence of elongated photoreceptor outer segments in central serous chorioretinopathy. Am J Ophthalmol [Internet]. 2011 Apr [cited 2020 Feb 24];151(4):617-623.e1. Available from: http://www.ncbi.nlm.nih.gov/pubmed/21257153
17. Maruko I, Iida T, Ojima A, Sekiryu T. Subretinal dot-like precipitates and yellow material in central serous chorioretinopathy. Retina [Internet]. 2011 Apr [cited 2020 Feb 24];31(4):759–65. Available from: http://www.ncbi.nlm.nih.gov/pubmed/21052035
18. Spaide RF, Klancnik JM. Fundus autofluorescence and central serous chorioretinopathy. Ophthalmology [Internet]. 2005 May [cited 2020 Feb 24];112(5):825–33. Available from: http://www.ncbi.nlm.nih.gov/pubmed/15878062
19. Bloom SM, Singal IP. The outer bruch membrane layer: A previously undescribed spectral-domain optical coherence tomography finding. Retina [Internet]. 2011 Feb [cited 2020 Feb 24];31(2):316–23. Available from: http://www.ncbi.nlm.nih.gov/pubmed/20890240
20. Xing LI, Yunlan LI ML. Optical coherence tomography in central serous choroidoretinopathy. CHINESE J Ocul FUNDUS Dis [Internet]. 1999 [cited 2020 Feb 24];(3):3. Available from: http://en.cnki.com.cn/Article_en/CJFDTotal-ZHYD199903000.htm
21. Lin D, Chen W, Zhang G, Huang H, Zhou Z, Cen L, et al. Comparison of the optical coherence tomographic characters between acute Vogt-Koyanagi-Harada disease and acute central serous chorioretinopathy. BMC Ophthalmol. 2014 Jun 28;14(1):87.
22. Montero JA, Ruiz-Moreno JM. Optical coherence tomography characterisation of idiopathic central serous chorioretinopathy. Br J Ophthalmol. 2005 May;89(5):562–4.
23. Kim HC, Cho W Bin, Chung H. Morphologic changes in acute central serous chorioretinopathy using spectral domain optical coherence tomography. Korean J Ophthalmol. 2012;26(5):347–54.
24. Jampol LM, Shankle J, Schroeder R, Tornambe P, Spaide RF, Hee MR. Diagnostic and Therapeutic Challenges. Retina [Internet]. 2006 Nov [cited 2020 Feb 24];26(9):1072–6. Available from: http://journals.lww.com/00006982-200611000-00015
25. Abe S, Yamamoto T, Kirii E, Yamashita H. Cup-shaped choroidal excavation detected by optical coherence tomography: A case report. Retin Cases Br Reports [Internet]. 2010 Sep [cited 2020 Feb 24];4(4):373–6. Available from: http://www.ncbi.nlm.nih.gov/pubmed/25390922
26. Wakabayashi Y, Nishimura A, Higashide T, Ijiri S, Sugiyama K. Unilateral choroidal excavation in the macula detected by spectral-domain optical coherence tomography. Acta Ophthalmol [Internet]. 2010 May [cited 2020 Feb 24];88(3):e87-91. Available from: http://www.ncbi.nlm.nih.gov/pubmed/20546234
27. Margolis R, Mukkamala SK, Jampol LM, Spaide RF, Ober MD, Sorenson JA, et al. The expanded spectrum of focal choroidal excavation. Arch Ophthalmol [Internet]. 2011 Oct [cited 2020 Feb 24];129(10):1320–5. Available from: http://www.ncbi.nlm.nih.gov/pubmed/21670327
28. Katome T, Mitamura Y, Hotta F, Niki M, Naito T. Two cases of focal choroidal excavation detected by spectral-domain optical coherence tomography. Case Rep Ophthalmol [Internet]. 2012 Jan [cited 2020 Feb 24];3(1):96–103. Available from: http://www.ncbi.nlm.nih.gov/pubmed/23008695
29. Kobayashi W, Abe T, Tamai H, Nakazawa T. Choroidal excavation with polypoidal choroidal vasculopathy: A case report. Clin Ophthalmol. 2012 Aug 24;6(1):1373–6.
30. Say EAT, Jani PD, Appenzeller MF, Houghton OM. Focal choroidal excavation associated with polypoidal choroidal vasculopathy. Ophthalmic Surg Lasers Imaging Retin [Internet]. 2013 Jul [cited 2020 Feb 24];44(4):409–11. Available from: http://www.ncbi.nlm.nih.gov/pubmed/23883536
31. Wang Y, Chen Z-Q, Wang W, Fang X-Y. Multimodal Imaging Evaluations of Focal Choroidal Excavations in Eyes with Central Serous Chorioretinopathy. J Ophthalmol. 2016;2016.
32. Liu GH, Lin B, Sun XQ, He ZF, Li JR, Zhou R, et al. Focal choroidal excavation: A preliminary interpretation based on clinic and review. Int J Ophthalmol. 2015 Jun 18;8(3):513–21.
33. Li B, Ye J, Zhang M, Li D. The fundus manifestations and SD-OCT findings of patients with acute Vogt-Koyanagi-Harada disease. Chinese J Ophthalmol. 2017 Jun 11;53(6):436–9.

34. Zhao GL, Li RZ, Pang YH, Wang XQ, Peng HJ, Wei JF, et al. Diagnostic function of 3D optical coherence tomography images in diagnosis of Vogt-Koyanagi-Harada disease at acute uveitis stage. Med Sci Monit. 2018 Feb 3;24:687–97.
35. Xi-Jia. ZX-M. HB-A. P. Characteristics of near infrared imaging in central serous chorioretinopathy. Rec Adv Ophthalmol. 2011;31:976–9.
36. Manjunath V, Taha M, Fujimoto JG, Duker JS. Choroidal thickness in normal eyes measured using cirrus HD optical coherence tomography. Am J Ophthalmol. 2010;150(3):325.

Figures

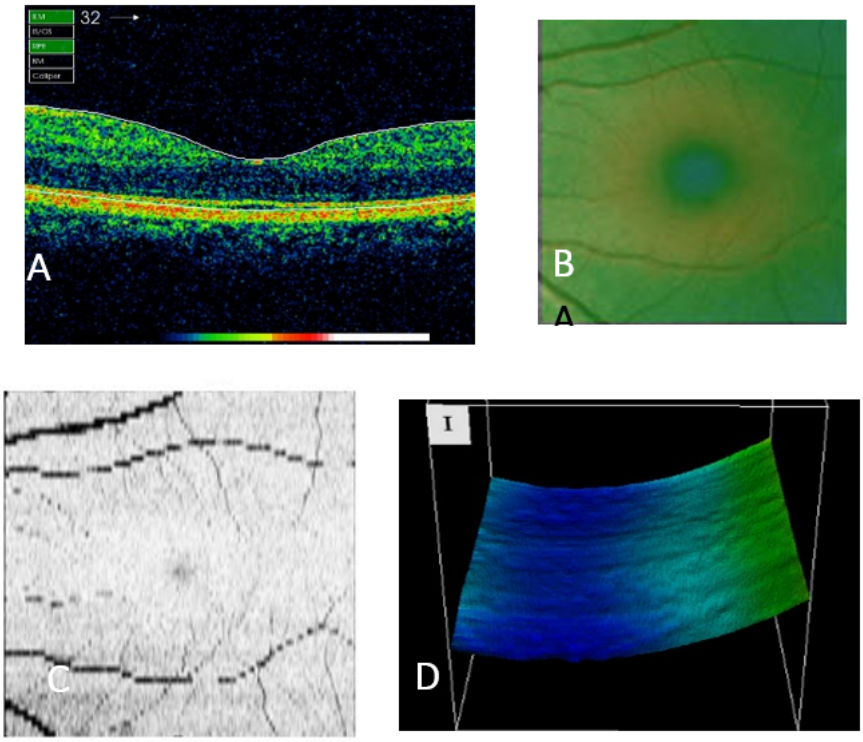

Figure 1

Normal 3D OCT image. The A diagram is a B-Scan diagram, ILM and PRE are marked with white lines, ILM-RPE thickness is the distance between the two lines. The B diagram is normal ILM-RPE map, which represents the macular thickness. The C diagram is the Shadowgram of OCT. It is white or gray, the blood vessels were clear, the central fovea was black dots, and the para fovea was brighter. The D diagram is the RPE Surface.

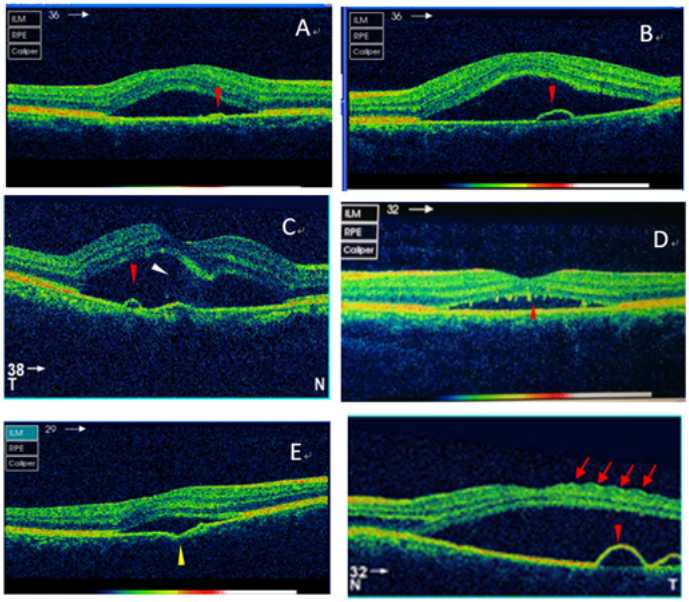

Figure 2

OCT image of CSC. The A diagram shows ERD, undivided retina are normal. Red arrowhead indicate small bulge in the RPE layer. The B diagram shows ERD, and the red arrowhead indicates PED. The white arrowhead in C diagram refers to the focal membranous reflection under ERD, and the corresponding position is PRE small convex, PED is visible next to it. The red arrowhead in the D diagram is ERD combined with Subretinal dot-like precipitates. E map shows ERD and FCE (Yellow arrowhead). The F diagram shows ERD and PED (red arrowhead), and FI (ILM) (red arrow).

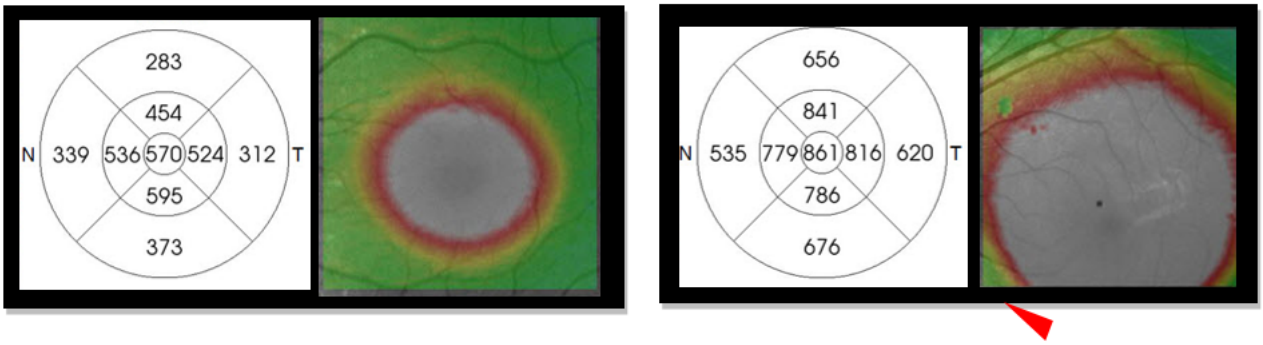

Figure 3

ILM-RPE thickness map of CSC. We can see a round dome. The left picture shows a single round dome in the range of 6 × 6 mm2 and the thickness of macular were express on the left grid. The right picture shows a single round dome is beyond the scope of examination. A small green circular change (red arrowhead) can be seen in the red lesions above the right picture and the thickness of macular were express on the left grid.

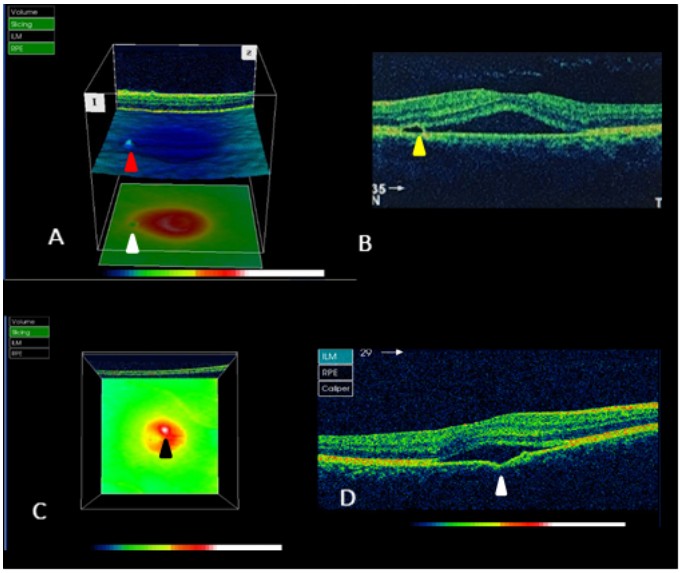

Figure 4

OCT image of CSC. The A diagram shows a small green round change at the left edge of the red lesion on the ILM-RPE thickness map (white arrowhead). The corresponding RPE surface shows a small focal bulge (red arrowhead). The B diagram is the B-Scan map of the same location, which shows that the green dot is a focal PED (yellow arrowhead). White dot-like changes(black arrowhead) were seen in the red lesions on the ILM-RPE thickness map on the C diagram, and the B-Scan image on the D diagram showed that the RPE was convex in the corresponding position (white arrowhead) and the ILM-RPE thickness increased.

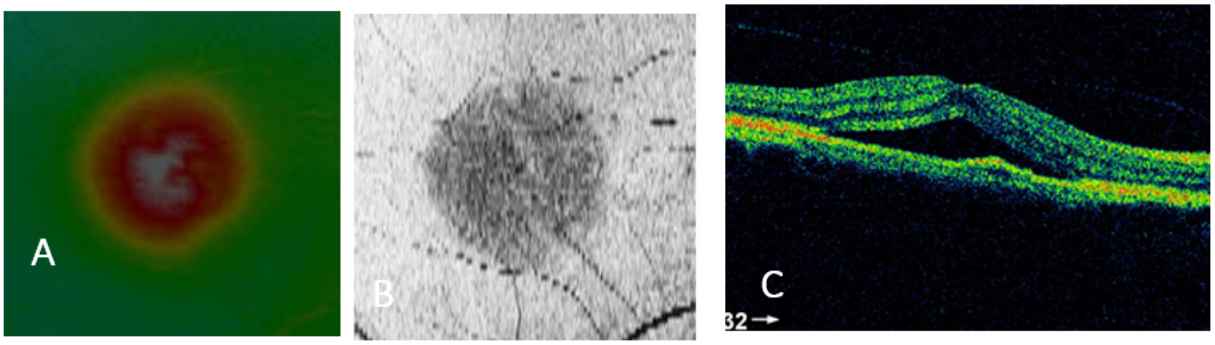

Figure 5

The A, B, C diagrams were from the same eye. On ILM-RPE map, we can see a round uniform dome (A) and in Shadowgram image, the eyes had a round black figure that correspond with dome In ILM-RPE thickness map (B). B-Scan images of the macular have EDR and small bulge (C).

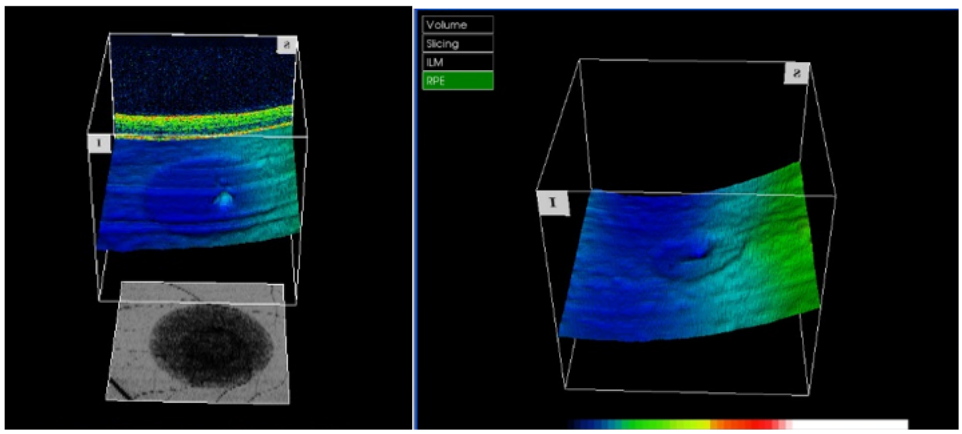

Figure 6

RPE surface of CSC. Right image shows a shallow plate depression with a focal uplift, and the shadowgram image correspond with it. The left image has a shallow plate depression with a central focal excavation.